Evaluation of spin polarization in p-$In_{0.96}Mn_{0.04}As$ using Andreev reflection spectroscopy including inverse proximity effect

Tatsushi Akazaki*
NTT Basic Research Laboratories, NTT Corporation, 3-1 Morinosato-Wakamiya, Atsugi, Kanagawa 243-0198, Japan

Takehito Yokoyama
Department of Physics, Tokyo Institute of Technology, 2-12-1 Ookayama, Meguro-ku, Tokyo 152-8550, Japan

Yukio Tanaka
Department of Applied Physics, Nagoya University, Furo-cho, Chikusa-ku, Nagoya 464-8603, Japan

Hiro Munekata
Imaging Science and Engineering Laboratory, Tokyo Institute of Technology, 4259-R2-57 Nagatsuta-cho, Midori-ku, Yokohama 226-8503, Japan

Hideaki Takayanagi†
Research Institute for Science and Technology, Tokyo University of Science, 1-3 Kagurazaka, Shinjuku, Tokyo 162-8601, Japan
(Received 27 April 2010; revised manuscript received 16 January 2011; published 29 April 2011)

We report on carrier transport across a superconductor/ferromagnetic semiconductor junction with a highly transparent metallic contact, Nb/p-$In_{0.96}Mn_{0.04}As$. Below ~10 K, p-$In_{0.96}Mn_{0.04}As$ becomes ferromagnetic, as evidenced by the hysteretic transverse resistance caused by the anomalous Hall effect. Below the superconducting critical temperature T_c of the Nb electrodes (8.2 K), a conductance reduction occurs within the bias voltage that is comparable to the Nb superconducting energy gap. A rather moderate slope in the differential conductance curves within the gap region indicates the partial suppression of the Andreev reflection caused by spin-polarized carriers in p-$In_{0.96}Mn_{0.04}As$. Spin polarization P in p-$In_{0.96}Mn_{0.04}As$ has been extracted by fitting the measured differential conductance curves with a newly modified Blonder-Tinkham-Klapwijk model with both spin polarization and the inverse proximity effect (mod2-BTK model). The extracted P value is $P = 0.725$ at 0.5 K, and it decreases gradually with increasing temperature.

DOI: 10.1103/PhysRevB.83.155212 PACS number(s): 72.25.Dc, 74.45.+c, 75.50.Pp

I. INTRODUCTION

Superconductor/ferromagnet (S-F) junctions have attracted considerable interest both theoretically and experimentally.[1] This is because new quantum phenomena can be expected from the interplay between the superconductivity and the spin polarization of the ferromagnet. This interplay allows us to determine experimentally the spin polarization of carriers P in a ferromagnet using Andreev reflection spectroscopy.[2–7] In contrast to the superconducting tunnel junction technique,[8,9] which is the most widely used method for determining P, Andreev reflection spectroscopy has the advantage of being able to measure P without the formation of a tunnel barrier. The underlying principle is as follows.[10] An incident electron has to be converted into a Cooper pair to enter the superconductor, for which an opposite spin electron has to be removed from the normal region. Therefore when there is no opposite spin electron in the normal region, no conversion occurs. Namely, with S-F junctions, the Andreev reflection is limited by the minority spin population. As a result, the Andreev reflection process is sensitive to the spin states of carriers in that the spin polarization greatly affects the Andreev reflection probability. This notion has been theorized by early workers[2,4] by decomposing the net current I into two parts $(1 - P)I_u$ and PI_p, and calculating the conductance curve on the basis of Blonder-Tinkham-Klapwijk (BTK) theory,[11] which we call hereafter the mod1-BTK model. Here, $(1 - P)I_u$ is the fully unpolarized current component for which Andreev reflection is allowed, whereas PI_p is the fully polarized current component for which Andreev reflection probability is zero. The P values in various ferromagnets,[2–4,7] including (Ga,Mn)As,[5] have been estimated by fitting the conductance spectrum with the mod1-BTK model and its relatives. An empirical approach with density-of-states broadening has also been used to extract the P value in (Ga,Mn)As.[6] However, it is inferred that, in an S-F junction, the pair potential Δ in a superconductor is weakened as a result of the penetration of the exchange field from a ferromagnet into a superconductor, which is called the inverse proximity effect.[12–14] This interesting deliberation has motivated us to study the influence of the inverse proximity effect on spin-polarized carrier transport across the S-F interface as well as the estimation of the P value.

In this paper, we are concerned with Andreev reflection spectroscopy across Nb/p-$In_{0.96}Mn_{0.04}As$ S-F junctions. As reported earlier,[5,6] III-V-based ferromagnetic semiconductors are assumed to exhibit half-metallic-like behavior at low temperatures. We have estimated the P values by fitting the measured differential conductance with a newly modified Blonder-Tinkham-Klapwijk model which incorporates both spin polarization and the inverse proximity effect (mod2-BTK model). The essential part of the modification is the introduction of the reduced pair potential near the S-F interface.

Consequently, we have found that the effect of the inverse proximity effect primarily manifests itself as a softening of the conductance slope in the superconductor gap region. We have obtained $P \sim 0.725$ at 0.5 K for p-$In_{0.96}Mn_{0.04}As$, which we believe is reliable and offers a benchmark for testing the theoretical picture of carrier-mediated ferromagnetism.

II. EXPERIMENTS AND DISCUSSIONS

The p-$In_{0.96}Mn_{0.04}As$ heterostructure was grown on a semi-insulating (001) GaAs substrate by using molecular beam epitaxy (MBE).[15] A GaSb (lattice constant $a_0 = 0.605$ nm) layer had to be deposited to accommodate the large lattice mismatch between the GaAs substrate ($a_0 = 0.565$ nm), the InAs epilayer ($a_0 = 0.608$ nm), and related alloy layers. In fact, carrier-mediated ferromagnetism in an InMnAs layer could be obtained only when appropriate buffer layers were placed between GaAs and InMnAs.[16] The drawback, which reflects the type-II band alignment at InAs/GaSb,[17] is that some of the holes in InMnAs are transferred to GaSb, and reside in the GaSb side of InMnAs/GaSb.[18] This gives rise to parallel conductance, and thus an overestimation of carrier mobility.

Figure 1 shows the magnetic-field dependence of the Hall resistance R_H for p-$In_{0.96}Mn_{0.04}As$ at 0.5 K, which was obtained using standard Hall bar geometry, as shown in Fig. 1(b). The slope of the R_H-H curve in high fields (10 000–90 000 G) allows us to estimate a carrier density n_h of 2.2×10^{19} cm^{-3}. Here, we should note that we disregard the possible contribution of parallel conduction on the GaSb side of an $In_{0.96}Mn_{0.04}As$/GaSb interface.[18] Using both n_h and the longitudinal resistance without a magnetic field, the mobility μ_h at 0.5 K is estimated to be 71 cm^2/V s.

The Nb/p-$In_{0.96}Mn_{0.04}As$ junctions were fabricated simply by depositing an ~80-nm-thick Nb layer on p-$In_{0.96}Mn_{0.04}As$, followed by a standard liftoff process. The device configurations incorporating both Nb superconductor and Ti/Au normal contact pads are shown in Figs. 2(a) and 3(a). No post-deposition procedure was necessary to realize ohmic characteristics for Nb/p-$In_{0.96}Mn_{0.04}As$, as anticipated from previous work on a Pt/Ti/p-InAs ohmic contact without annealing.[19] Ohmic contact characteristics have also been established for the Nb/n-InAs system.[20,21] The critical temperature T_c of the Nb electrodes was about 8.2 K.

Figure 2(b) shows the R_H-H curves in low fields obtained at various temperatures from the device shown in Fig. 2(a). The measurement setup is also shown in Fig. 2(a). The overall R_H is expressed by[22–25]

$$R_H = R_0 B + R_S M, \tag{1}$$

where $R_0 B$ and $R_S M$ are ordinary and anomalous Hall resistance terms, respectively. A small portion of the sample resistance component (R_{xx}), which was superimposed on the raw Hall resistance component (R_{xy}), has been removed by employing the even/odd function separation method.[22] Since the anomalous Hall resistance term is dominant in low fields, the R_H curve exhibits a square hysteresis loop, reflecting the magnetization (M-H) curve of a ferromagnetic p-$In_{0.96}Mn_{0.04}As$ layer. At 20 K, the Hall resistance curve exhibits linear behavior, whereas it becomes nonlinear at 15 K. Clear hysteretic behavior develops at 10 K with remnant Hall

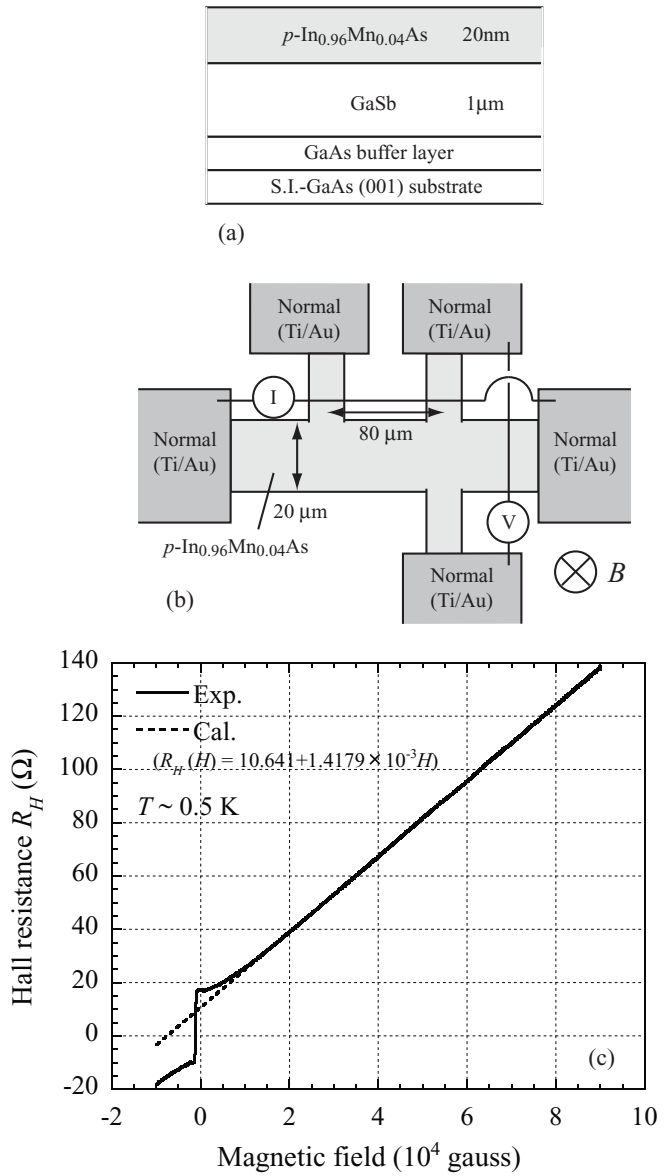

FIG. 1. (a) Schematic cross-sectional view of a p-$In_{0.96}Mn_{0.04}As$ wafer, (b) a Hall bar and measurement setup, and (c) magnetic-field dependence of Hall resistance for p-$In_{0.96}Mn_{0.04}As$. The applied magnetic fields range from +90 000 to −10 000 G.

resistance. These facts indicate that the Curie temperature is between 10 and 15 K, and the film has an out-of-plane magnetization easy axis. Therefore the Nb/p-$In_{0.96}Mn_{0.04}As$ junction can be considered an S-F junction below the T_c of the Nb electrodes (8.2 K).

A nonlocal measurement technique consisting of a three-terminal configuration [Fig. 3(a)] has been employed to detect the Nb/p-$In_{0.96}Mn_{0.04}As$ interface resistance. We let a charge current flow from the upper Nb electrode to the left Ti/Au electrode placed at the left end of the p-$In_{0.96}Mn_{0.04}As$ slab, and measured the voltage of the upper Nb electrode with respect to the right Ti/Au electrode placed at the right end of the p-$In_{0.96}Mn_{0.04}As$ slab. Two Ti/Au electrodes were connected to the same ground. Electric potential of the p-$In_{0.96}Mn_{0.04}As$ region adjacent to the upper Nb electrode is supposed to be nearly equal to that of the right Ti/Au electrode, since

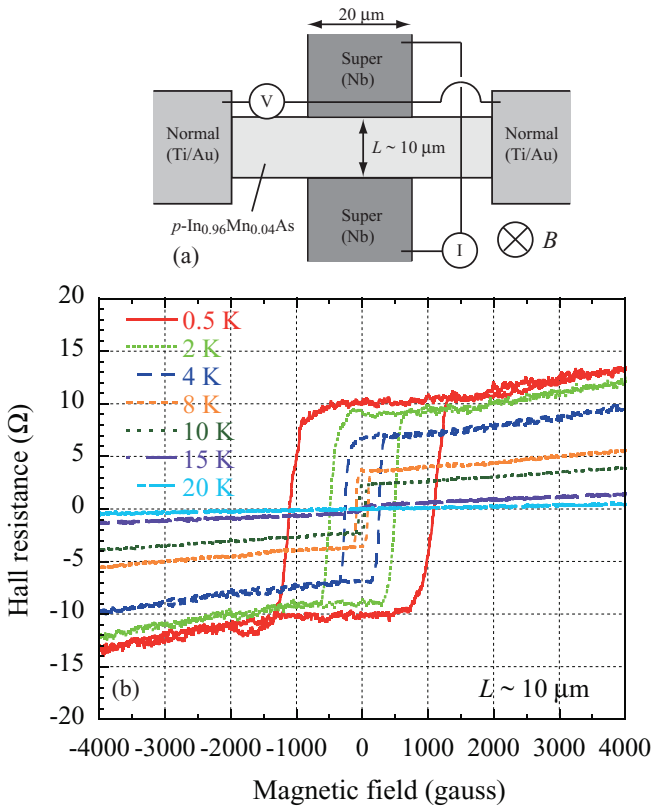

FIG. 2. (Color online) (a) Measurement setup and (b) Hall resistance curves obtained from the setup shown in (a) at various temperatures.

no current flows across the right half of the slab. Therefore the voltage obtained by the measurement is regarded as the voltage drop across the Nb/p-$In_{0.96}Mn_{0.04}As$ interface. The normal-state resistance measured in this fashion was 2.3 kΩ at 0.5 K at the bias voltage of $V = 2$ mV.

The dI/dV-V characteristics of a double Nb/p-$In_{0.96}Mn_{0.04}As$ junction measured between the upper and lower Nb electrodes with four-terminal measurement looked almost the same as those of a single Nb/p-$In_{0.96}Mn_{0.04}As$ junction [Fig. 3(b)], except for the double bias voltage. The normal-state resistance was around 4.8 kΩ, which was twice as large as that measured for the single junction. Knowing that the estimated resistance of the central p-$In_{0.96}Mn_{0.04}As$ channel of 20 μm (width) × 0.8 μm (length) × 20 nm (thickness) is 80 Ω, we are able to infer that resistance measured across the double S-F junction primarily consists of a series of two Nb/p-$In_{0.96}Mn_{0.04}As$ single junctions.

In the case of a planar-type junction, a current between Nb and p-$In_{0.96}Mn_{0.04}As$ primarily flows through the edge part of a Nb electrode because it prefers to flow within a superconducting Nb electrode. The effective contact area at the edge of the Nb electrode is estimated to be 4×10^{-9} cm^2 [20 μm long (Nb) × 20 nm thick (p-$In_{0.96}Mn_{0.04}As$)], yielding the contact resistance of around 1×10^{-5} Ω cm^2. This value is four orders of magnitude lower than the contact resistance of a Ga/p-$Ga_{1-x}Mn_xAs$ junction[5] whose interface resistance was 10–100 Ω with a contact area of 1 mm × 1 mm. Therefore we believe that the contact resistance, and thus the barrier scattering parameter Z of our Nb/p-$In_{0.96}Mn_{0.04}As$ interface, is sufficiently low to study carrier transport across the interface.

Let us now return to the dI/dV-V characteristics of a Nb/p-$In_{0.96}Mn_{0.04}As$ junction, as shown in Fig. 3(b). The dI/dV-V characteristics exhibit almost no voltage dependence above the T_c of Nb. Below the T_c of Nb, we obtained a conductance reduction within ∼±1.5 mV. The magnitude of the conductance reduction gradually increased as the temperature decreased. Taking the typical Nb superconducting energy gap of ∼1.5 meV into account, we suppose that this conductance reduction appears within the superconducting gap. Moreover, there were almost no conductance peaks near ∼±1.5 mV. These features suggest that the Nb/p-$In_{0.96}Mn_{0.04}As$ junction has a highly transparent metallic contact with a low barrier scattering parameter at the S-F interface. This feature is also noticeable in data obtained in studies of (Ga,Mn)As.[5,6] For junctions consisting of materials with a Fermi velocity mismatch, the *effective* Z value can be expressed by[26]

$$Z = \left[Z_i^2 + \frac{(1-r)^2}{4r} \right]^{1/2}, \qquad (2)$$

where Z_i is the intrinsic barrier scattering parameter at the S-F interface, and $r = v_{F,F}/v_{F,S}$ is the ratio of the Fermi velocity. Taking account of the values $v_{F,S} = 1.37 \times 10^8$ cm/s for Nb[27] and $v_{F,F} = 8.3 \times 10^7$ cm/s for p-$In_{0.96}Mn_{0.04}As$ derived from the measured carrier density $n_h = 2.2 \times 10^{19}$ cm^{-3} and hole effective mass $m_h = 0.12 m_0$,[28] we obtain an r value of 0.61.

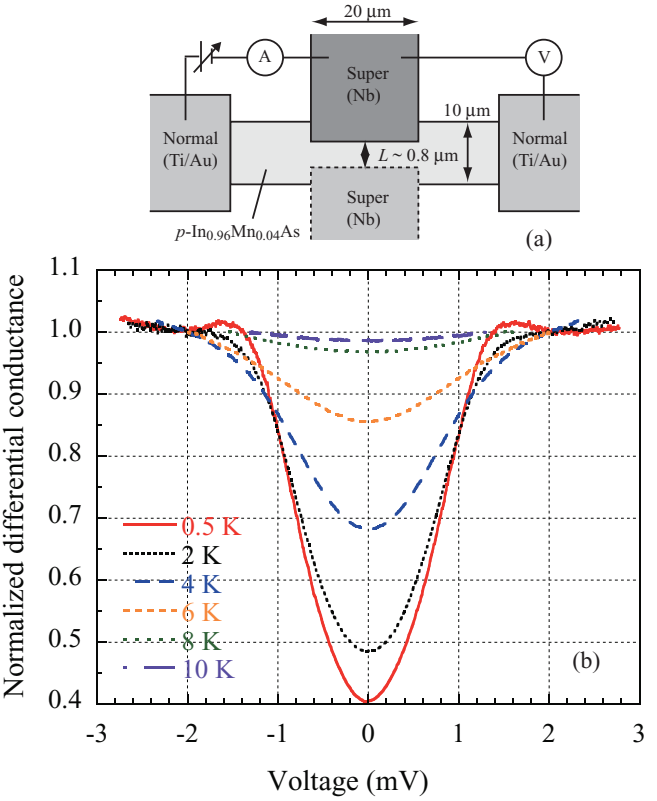

FIG. 3. (Color online) (a) Measurement setup and (b) normalized dI/dV-V characteristics obtained from the device shown in (a) at various temperatures.

Consequently, a Z value of 0.25 is derived assuming $Z_i = 0$ (an S-F interface without a tunneling barrier) and $r = 0.61$. This sufficiently low Z value suggests that our experimental results can be understood qualitatively by considering the suppression of the Andreev reflection caused by the spin polarization in p-$In_{0.96}Mn_{0.04}As$. We also measured the bias voltage dependence of the differential conductance after cooling without a magnetic field. There was little difference between the dependence measured after cooling without a magnetic field (magnetization in the virgin state) and that measured at a zero magnetic field after the sample had been magnetized. We conjecture that the microscopic magnetization in each magnetic domain contributes to the inverse proximity effect because the magnetic domain size is greater than the superconducting coherence length.

Having observed the suppressed Andreev reflection in an S-F junction, we now discuss the estimation of the spin polarization P in p-$In_{0.96}Mn_{0.04}As$. To estimate the P value in p-$In_{0.96}Mn_{0.04}As$ accurately with Andreev reflection spectroscopy, we must consider both the spin polarization and the inverse proximity effect. We do this with a fit to the differential conductance obtained with a newly modified BTK model incorporating both spin polarization and the inverse proximity effect.[12–14] Let us assume a Cooper pair near the S-F interface where one electron of the pair is in the superconductor, while the other is in the ferromagnet. In this case, it is preferable for the spin of the electron in the ferromagnet to be parallel to the majority of the spins in the ferromagnet. At the same time, the spin of the other electron in the superconductor must be opposite to the first one owing to spin-singlet pairing. This induces an effective magnetic field in the superconductor region whose direction is antiparallel to the field in the ferromagnet. Consequently, the pair potential Δ in the superconductor near the S-F interface is weakened. To extend the mod1-BTK model by including the inverse proximity effect, we must consider the effect of the gradual variation in Δ in the superconductor near an S-F interface. Here, the thickness of the Nb electrodes ($\sim$80 nm) is sufficiently less than the lateral Nb geometry (20 μm in width $\times$ $\sim$100 μm in length). Therefore we are able to neglect the out-of-plane pair potential distribution and simply consider the in-plane one. In accordance with van Son's method, which extends the BTK theory to study the effect of a gradual variation in Δ near the S-N interface,[29] we have extended the mod1-BTK model including the inverse proximity effect with the gradual variation in Δ near the S-F interface. Δ is zero in the ferromagnet and, at the S-F interface, increases in a steplike fashion, keeps increasing exponentially toward the bulk Nb within the penetration length of the exchange field X_P, and saturates with the intrinsic value of Nb in the Nb bulk, as shown schematically in the inset of Fig. 4. Here, Δ_S is the pair potential of bulk Nb, and Δ_{S0} is the pair potential at the S-F interface. In addition, we take into account the statistical distribution of Δ at the S-F interface since the interfacial roughness weakens specularity and thus degrades the uniformity of the inverse proximity effect: namely, Δ_{S0} assumes the Gaussian distribution $[\frac{1}{\sqrt{2\pi\sigma^2}}\exp(-\frac{(\Delta_{S0}-\mu)^2}{2\sigma^2})]$. The values of mean μ and variance σ^2 used in the model calculation are shown in the Fig. 4 caption. As shown in the

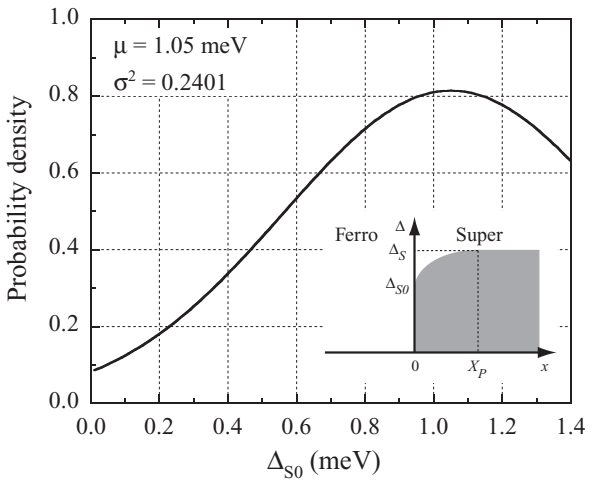

FIG. 4. Calculated probability distribution for the pair potential at the S-F interface Δ_{S0} assuming a Gaussian distribution $[\frac{1}{\sqrt{2\pi\sigma^2}}\exp(-\frac{(\Delta_{S0}-\mu)^2}{2\sigma^2})]$ with a mean μ of 1.05 meV and a variance σ^2 of 0.2401. The inset shows a schematic model of the system where the pair potential in the S region decreases exponentially near the S-F interface $[\Delta(0 \leqslant x \leqslant X_P) = (\Delta_S - \frac{(\Delta_S-\Delta_{S0})}{1-e}) + (\frac{(\Delta_S-\Delta_{S0})}{1-e})\exp(-\frac{(x-X_P)}{X_P})]$, whereas the pair potential vanishes in the F region.

Appendix, we found that a reasonable value for X_P is around 0.6 μm, suggesting that the spins in Nb survive over a much longer distance than the superconducting coherence length of $\sim$40 nm.[30] Note that, very recently, Yang *et al.* reported that the lifetime of spins in the superconducting state is about a million times longer than that in the normal conducting state.[31] Therefore we believe that it is reasonable for the characteristic length scale to be the spin-decay length of about 0.6 μm.

The Andreev reflection probabilities $A(E)$ and the normal reflection probabilities $B(E)$ are calculated by integrating the Bogoliubov–de Gennes equation based on van Son's method. $A(E)$ and $B(E)$ are represented by $A(E) = |a_e|^2$ and $B(E) = |b_e|^2$, respectively. Here, the coefficients a_e and b_e are the amplitudes of the Andreev reflected wave and the ordinary reflected wave, respectively, for an incident electron wave with amplitude 1. These coefficients are given by

$$a_e = \frac{u(0)v(0)}{(1+Z^2)u(0)^2 - Z^2v(0)^2},$$
$$b_e = \frac{iZ(1-iZ)(v(0)^2 - u(0)^2)}{(1+Z^2)u(0)^2 - Z^2v(0)^2}, \tag{3}$$

where $u(0)$ and $v(0)$ are the complex values at $x = 0$, which corresponds to the S-F interface. The values of $u(0)$ and $v(0)$ are governed by the following Bogoliubov–de Gennes equation where higher-order terms are neglected:

$$\frac{\partial u(x)}{\partial x} = i(\pi\xi_S\Delta_S)^{-1}\left[(E+i\Gamma)u(x) - \Delta(x)v(x)\right],$$
$$\frac{\partial v(x)}{\partial x} = -i(\pi\xi_S\Delta_S)^{-1}\left[(E+i\Gamma)v(x) - \Delta(x)u(x)\right]. \tag{4}$$

Here, E is the energy from the Fermi level, and Γ is the additional energy term resulting from the finite quasiparticle

lifetime effect.[32] Very recently, Kiss *et al.* determined a Γ value of 0.1–0.2 meV in Nb by using laser-excited ultrahigh-resolution photoemission spectroscopy.[33] Therefore we use $\Gamma = 0.15$ meV. ξ_S is the BCS coherence length of Nb, and $\Delta(x)$ is the spatially varying pair potential. The total current I through the S-F junction as a function of the bias voltage is given by

$$I \propto \int_{-\infty}^{\infty} [f(E-V,T) - f(E,T)][1 + A(E) - B(E)]\,dE, \tag{5}$$

where $f(E)$ is the Fermi-Dirac distribution function. According to the mod1-BTK model, I consists of two parts:

$$I = (1-P)I_u + PI_p, \tag{6}$$

where $(1-P)I_u$ is the fully unpolarized part of the current where Andreev reflection is allowed, and PI_p is the fully polarized part of the current where $A(E)$ is zero. I_u and I_p, respectively, are calculated by solving Eq. (5) with the above calculated $A(E)$ and $B(E)$ values based on van Son's method. The dI/dV-V curve can then be calculated by differentiating Eq. (6) as a function of the applied bias voltage V. The P value, which is a fitting parameter, must be determined to obtain the best fit between the calculated and measured differential conductance.

In Fig. 5, we compare measured and calculated dI/dV-V curves, and point out the importance of incorporating the inverse proximity effect. All the curves shown in the figure are normalized at a bias voltage of ~2 mV. The values of the physical quantities used for successful calculations are given in the Fig. 5 caption. The values of Z, Δ_S, and ξ_S were used for both the mod1-BTK and mod2-BTK calculations. Of these three quantities, well-accepted values were used for Δ_S and ξ_S, whereas the Z value was determined explicitly using Eq. (2) with the measured carrier concentration in a InMnAs layer [Fig. 1(c)]. The conventional calculation reproduces the magnitude of the relative change in junction conductance between zero-bias and saturation-bias (±2 mV) voltages with spin polarization $P = 0.745$. However, it is clear that the mod1-BTK model cannot reproduce the feature of gradually increasing conductance within the superconductor gap region; see the Appendix for details. As regards the calculated curve with the mod2-BTK model, the conductance-voltage characteristics within the gap region have been reproduced by properly adjusting the three parameters X_P, μ, and σ^2. Consequently, $P = 0.725$ was extracted as the optimal value for fitting. From the model calculation, we are able to state that the influence of the above three fitting parameters on the process for determining P is much smaller than we anticipated at the initial stage of the present work. It also becomes clear that the entire dI/dV-V curve, in particular, the softening observed in the conductance valley, can be well explained by taking account of the inverse proximity effect. Additional parameters introduced in the new model are the penetration length of the exchange field X_P, the Γ value, which is the quantity associated with inelastic scattering caused by imperfections within a Nb film, and two parameters μ and σ^2, which represent the inhomogeneity of the pair potential at the S-F interface in the form of Gaussian statistics. The results of calculations with different parameter values can be found in the Appendix. From these calculations, we can conclude that the Z value is the primary influence on the estimation of the P value. In contrast, the additional parameters of the inverse proximity effect, X_P, μ, and σ^2, suppress the abrupt feature of the Andreev reflection spectrum. We also note that results obtained earlier for Ga/GaMnAs (Ref. 5) and Sn/GaMnAs (Ref. 6) should be revisited with our model.

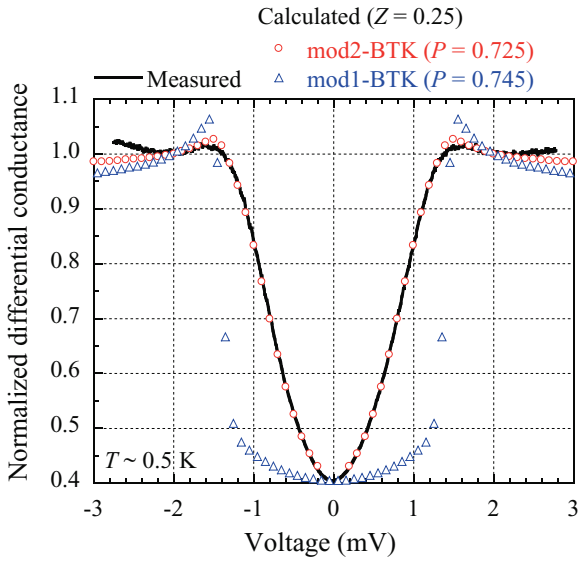

FIG. 5. (Color online) Comparison of the measured and calculated dI/dV-V characteristics at 0.5 K. The thick solid line (black) represents experimental data. The open circles (red) are calculated using the mod2-BTK model. The values used in the calculation are $Z = 0.25$, $P = 0.725$, $\Delta_S = 1.4$ meV, $\Gamma = 0.15$ meV, $\xi_S = 40$ nm, $X_P = 0.6$ μm, $\mu = 1.05$ meV, and $\sigma^2 = 0.2401$. The open triangles (blue) use the mod1-BTK model with $Z = 0.25$ and $P = 0.745$. dI/dV is normalized by the value near $V = 2$ mV.

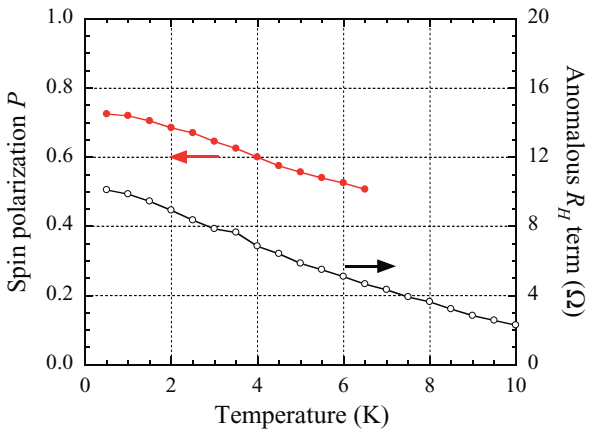

FIG. 6. (Color online) Temperature dependence of spin polarization P and anomalous Hall resistance terms in p-$In_{0.96}Mn_{0.04}As$. The solid circles (red) and left axis represent P. The open circles (black) and right axis represent anomalous Hall resistance terms. The P values are determined by comparing the measured dI/dV-V characteristics at several temperatures with those obtained from the mod2-BTK model. The anomalous Hall resistance terms are obtained from the y intercept of the R_H-H curves shown in Fig. 2(b).

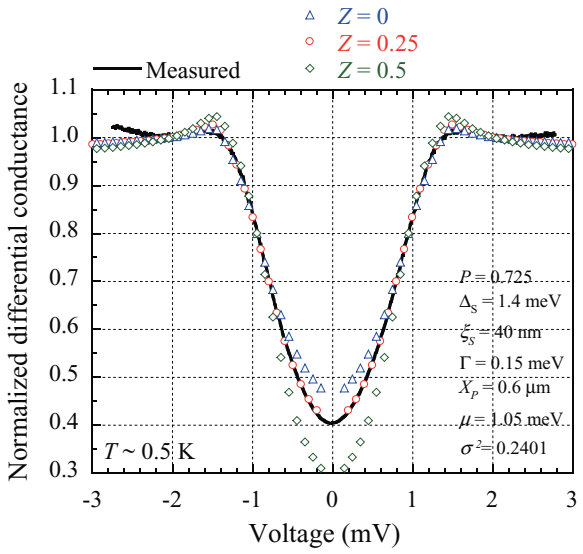

FIG. 7. (Color online) Calculated dI/dV-V characteristics at 0.5 K obtained using the mod2-BTK model with three different Z values. Open triangles (blue), open circles (red), open diamonds (green) indicate results obtained with $Z = 0$, 0.25, and 0.5, respectively. The thick solid line (black) represents experimental data obtained at 0.5 K. The dI/dV values are normalized with the value obtained at a bias voltage of $V = 2$ mV. Other physical quantities used for the calculations are $P = 0.725$, $\Delta_S = 1.4$ meV, $\Gamma = 0.15$ meV, $\xi_S = 40$ nm, $X_P = 0.6$ μm, $\mu = 1.05$ meV, and $\sigma^2 = 0.2401$, as shown in the inset.

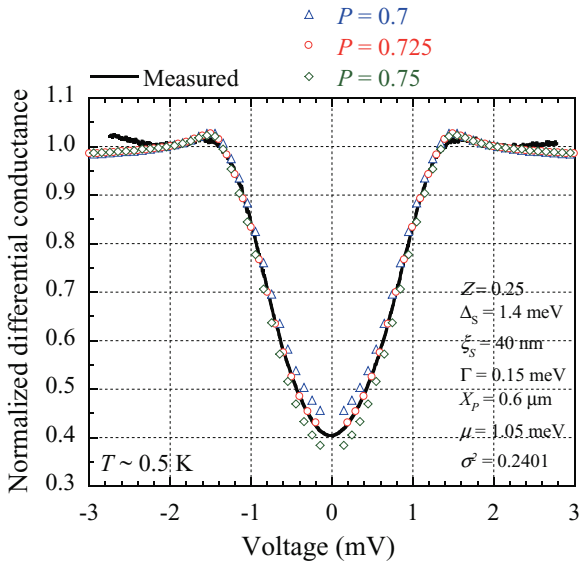

FIG. 8. (Color online) Calculated dI/dV-V characteristics at 0.5 K obtained using the mod2-BTK model with three different P values. Open triangles (blue), open circles (red), open diamonds (green) indicate results obtained with $P = 0.7$, 0.725, and 0.75, respectively. The thick solid line (black) represents experimental data obtained at 0.5 K. The dI/dV values are normalized with the value obtained at a bias voltage of $V = 2$ mV. Other physical quantities used for the calculations are $Z = 0.25$, $\Delta_S = 1.4$ meV, $\Gamma = 0.15$ meV, $\xi_S = 40$ nm, $X_P = 0.6$ μm, $\mu = 1.05$ meV, and $\sigma^2 = 0.2401$, as shown in the inset.

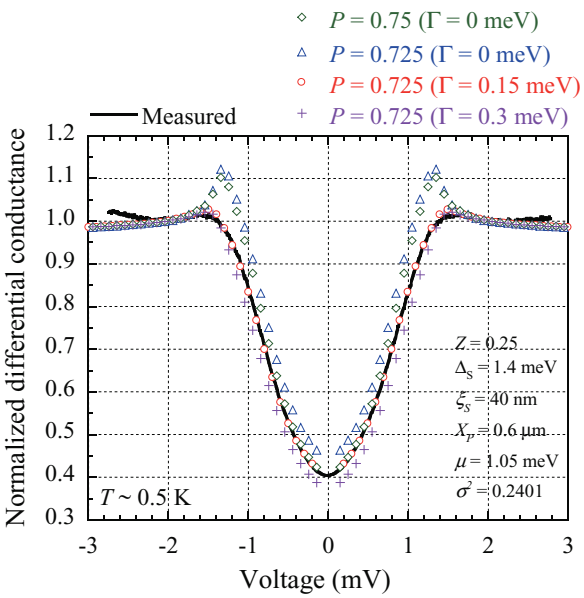

FIG. 9. (Color online) Calculated dI/dV-V characteristics at 0.5 K obtained using the mod2-BTK model using four different combinations of Γ and P values. Open diamonds (green) indicate results obtained with $\Gamma = 0$ meV and $P = 0.75$. Open triangles (blue), open circles (red), crosses (purple) indicate results obtained with $\Gamma = 0$, 0.15, 0.3 meV, and $P = 0.725$, respectively. The thick solid line (black) represents experimental data obtained at 0.5 K. The dI/dV values are normalized with the value obtained at a bias voltage of $V = 2$ mV. Other physical quantities used for the calculations are $Z = 0.25$, $\Delta_S = 1.4$ meV, $\xi_S = 40$ nm, $X_P = 0.6$ μm, $\mu = 1.05$ meV, and $\sigma^2 = 0.2401$, as shown in the inset.

Let us consider the effect of parallel conduction on the estimation of the P value. Recall that this problem is due to the GaSb channel at the p-$In_{0.96}Mn_{0.04}As$/GaSb interface,[18] and should be taken care of, since parallel conduction gives rise to an underestimation of the carrier concentration in a p-$In_{0.96}Mn_{0.04}As$ layer. Within the limit of $n_h < 10^{20}$ cm^{-3}, the r and Z values in Eq. (2) become closer to 1 and 0, respectively, as long as the relation $v_{F,F} \leqslant v_{F,S}$ is fulfilled. The condition $v_{F,F} = v_{F,S}$ gives the upper bound value of $n_h = 10^{20}$ cm^{-3}, with which we obtain $P = 0.77$. These facts indicate that the parallel conduction at the $In_{0.96}Mn_{0.04}As$/GaSb interface would not have a severe impact on the reliability of the P value.

Figure 6 shows the temperature dependence of P and the anomalous Hall resistance terms in p-$In_{0.96}Mn_{0.04}As$. The Curie temperature is 10 K or slightly higher as exemplified in the Hall data shown in Fig. 2(b). The temperature dependence of the anomalous Hall resistance terms corresponds to that of magnetization as long as the sheet resistance R_S is assumed to be nearly constant below the Curie temperature of ~10 K. We found that the P value decreases with increasing temperature, which is qualitatively consistent with the temperature dependence of magnetization. The temperature dependence of the P value can be understood in terms of hole-mediated ferromagnetism.[34] The low Curie temperature manifests itself in a small exchange splitting at the top of the valence band around which the Fermi level resides. When the sample temperature is increased, the exchange splitting presumably

closes up rapidly at elevated temperatures, especially near the Curie temperature. In other words, the imbalance in the hole population between the spin-up and spin-down states is reduced to a great extent when a sample is close to the Curie temperature. Other samples with higher Curie temperatures should be tested in future work. The P value of 0.725 in p-$In_{0.96}Mn_{0.04}As$ at 0.5 K is lower than that of ~0.85 in p-$Ga_{1-x}Mn_xAs$ ($x = 0.05$ or 0.08).[5,6] Nevertheless, it is interesting to note that both systems have relatively high P values, which is probably one of the intrinsic characteristics of III-V ferromagnetic semiconductors.

III. CONCLUSION

We have studied spin-polarized carrier transport across Nb/p-$In_{0.96}Mn_{0.04}As$ junctions. We have observed that subgap conductance is suppressed, and that conductance peaks near the bias voltage of $V = \pm\Delta/e$ are strongly smeared out. These experimental results indicate highly transparent metallic contact between Nb and p-$In_{0.96}Mn_{0.04}As$ with a high P value. The moderate slope of a dI/dV-V curve in the subgap region can be understood by considering the suppression of the Andreev reflection caused by the spin polarization in p-$In_{0.96}Mn_{0.04}As$. We have evaluated the P values in p-$In_{0.96}Mn_{0.04}As$ experimentally by comparing the measured differential conductance with that calculated by a newly modified BTK model including both spin polarization and the inverse proximity effect. Consequently, the P value extracted experimentally for p-$In_{0.96}Mn_{0.04}As$ at 0.5 K has been $P = 0.725$ with $Z = 0.25$.

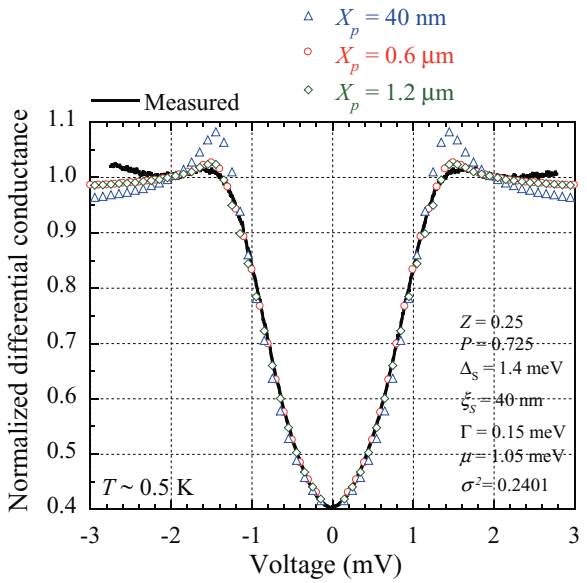

FIG. 10. (Color online) Calculated dI/dV-V characteristics at 0.5 K obtained using the mod2-BTK model with three different X_P values. Open triangles (blue), open circles (red), open diamonds (green) indicate results obtained with $X_P = 40$ nm, 0.6 μm, and 1.2 μm, respectively. The thick solid line (black) represents experimental data obtained at 0.5 K. The dI/dV values are normalized with the value obtained at a bias voltage of $V = 2$ mV. Other physical quantities used for the calculations are $Z = 0.25$, $P = 0.725$, $\Delta_S = 1.4$ meV, $\Gamma = 0.15$ meV, $\xi_S = 40$ nm, $\mu = 1.05$ meV, and $\sigma^2 = 0.2401$, as shown in the inset.

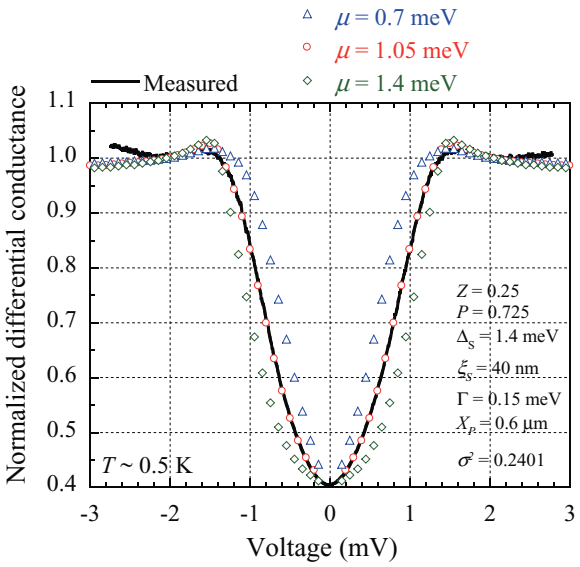

FIG. 11. (Color online) Calculated dI/dV-V characteristics at 0.5 K obtained using the mod2-BTK model with three different μ values. Open triangles (blue), open circles (red), open diamonds (green) indicate results obtained with $\mu = 0.7$, 1.05, and 1.4 meV, respectively. The thick solid line (black) represents experimental data obtained at 0.5 K. The dI/dV values are normalized with the value obtained at a bias voltage of $V = 2$ mV. Other physical quantities used for the calculations are $Z = 0.25$, $P = 0.725$, $\Delta_S = 1.4$ meV, $\Gamma = 0.15$ meV, $\xi_S = 40$ nm, $X_P = 0.6$ μm, and $\sigma^2 = 0.2401$, as shown in the inset.

ACKNOWLEDGMENTS

We thank J. Nitta, A. A. Golubov, Y. Asano, T. Kiss, and T. Noguchi for valuable discussions. We also thank H. Yamaguchi for his encouragement throughout this work. We are grateful to T. Schallenberg for sample preparation. This work was supported in part by a Grant-in Aid for Scientific Research on Innovative Areas "Topological Quantum Phenomena" from MEXT of Japan. H.M. acknowledges partial support from Grant-in-Aid for Scientific Research No. 19048020 and Advanced Photon Science Alliance Project, both from MEXT.

APPENDIX: RESULTS OF CALCULATIONS WITH DIFFERENT PARAMETER VALUES

The purpose of this Appendix is to clarify the cause and effect in relation to the calculated dI/dV-V characteristics and physical quantities Z, P, Γ, X_P, μ, and σ^2. It has become clear from these calculations that X_P, μ, and σ^2 have little influence on the process of determining the P value, and rather appear in the overall shape of dI/dV-V curves, in particular, in the softening of the conductance valley and the peaks appearing at the valley edges.

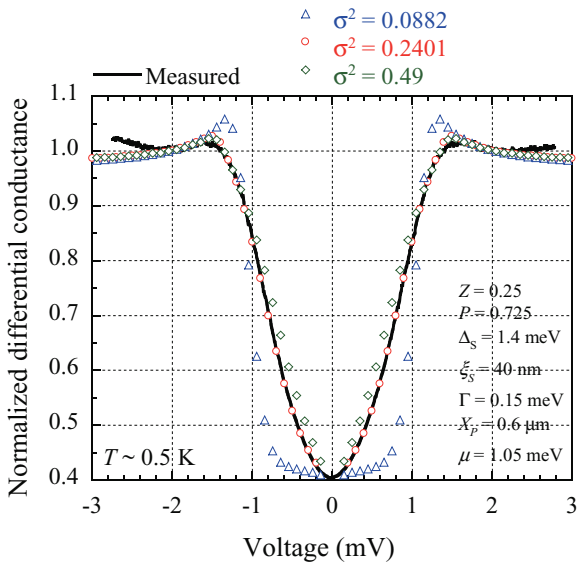

FIG. 12. (Color online) Calculated dI/dV-V characteristics at 0.5 K obtained using the mod2-BTK model with three different σ^2 values. Open triangles (blue), open circles (red), open diamonds (green) indicate results obtained with $\sigma^2 = 0.0882$, 0.2401, and 0.49, respectively. The thick solid line (black) represents experimental data obtained at 0.5 K. The dI/dV values are normalized with the value obtained at a bias voltage of $V = 2$ mV. Other physical quantities used for the calculations are $Z = 0.25$, $P = 0.725$, $\Delta_S = 1.4$ meV, $\Gamma = 0.15$ meV, $\xi_S = 40$ nm, $X_P = 0.6$ μm, and $\mu = 1.05$ meV, as shown in the inset.

In Figs. 7 and 8 we show the dependence of Z and P on the dI/dV-V characteristics, respectively. The other physical quantities are fixed at their optimal values to yield the best fit between the calculated and measured differential conductance. The difference between the dI/dV values for the zero-bias and normal conductance states is the primary quantity that affects both Z and P.[2,4,5]

In Fig. 9 we show the calculated dI/dV-V characteristics with various combinations of Γ and P values. Fixing the P value at $P = 0.725$, we find that the best fit is obtained with $\Gamma = 0.15$ meV. When Γ is set at $\Gamma = 0$, $P = 0.75$ is found to be the optimum value. However, conductance peaks appear near $\sim\pm 1.4$ mV, reflecting the effect of Δ_S. Consequently, we find that the overall dI/dV-V characteristics cannot be reproduced without setting a finite value for Γ.

In Fig. 10, we show the calculated dI/dV-V characteristics with three different X_P values, including $X_P = 40$ nm, which is equal to the superconducting coherent length (ξ_S) in Nb. The experimental dI/dV-V curve can be reproduced with $X_P = 40$ nm for the valley region ($|V| \leqslant 1.4$ mV), whereas there is a severe discrepancy at the peak regions near $\sim\pm 1.4$ mV with $X_P = 40$ nm.

Figures 11 and 12 show the calculated dI/dV-V characteristics with various μ and σ^2 values, respectively. It is clearly seen that μ and σ^2 primarily influence the overall shape of the dI/dV-V characteristics. In all cases, $P = 0.725$ was extracted as the optimum value after fitting.

*akazaki@will.brl.ntt.co.jp
†Also at International Center for Materials Nanoarchitectonics, NIMS, 1-2-1 Sengen, Tsukuba, Ibaraki, 305-0003, Japan.

[1]For example, *Nanoscale Devices—Fundamentals and Applications*, edited by R. Gross, A. Sidorenko, and L. Tagirov, NATO Science Series II: Mathematics, Physics and Chemistry Vol. 233 (Springer, Dordrecht, 2006).
[2]R. J. Soulen Jr., J. M. Byers, M. S. Osofsky, B. Nadgorny, T. Ambrose, S. F. Cheng, P. R. Broussard, C. T. Tanaka, J. Nowak, J. S. Moodera, A. Barry, and J. M. D. Coey, Science **282**, 85 (1998).
[3]S. K. Upadhyay, A. Palanisami, R. N. Louie, and R. A. Buhrman, Phys. Rev. Lett. **81**, 3247 (1998).
[4]G. J. Strijkers, Y. Ji, F. Y. Yang, C. L. Chien, and J. M. Byers, Phys. Rev. B **63**, 104510 (2001).
[5]J. G. Braden, J. S. Parker, P. Xiong, S. H. Chun, and N. Samarth, Phys. Rev. Lett. **91**, 056602 (2003).
[6]R. P. Panguluri, K. C. Ku, T. Wojtowicz, X. Liu, J. K. Furdyna, Y. B. Lyanda-Geller, N. Samarth, and B. Nadgorny, Phys. Rev. B **72**, 054510 (2005).
[7]F. Pérez-Willard, J. C. Cuevas, C. Surgers, P. Pfundstein, J. Kopu, M. Eschrig, and H. v. Löhneysen, Phys. Rev. B **69**, 140502(R) (2004).
[8]P. M. Tedrow and R. Meservey, Phys. Rev. Lett. **26**, 192 (1971).
[9]R. Meservey and P. M. Tedrow, Phys. Rep. **238**, 173 (1994).
[10]M. J. M. de Jong and C. W. J. Beenakker, Phys. Rev. Lett. **74**, 1657 (1995).
[11]G. E. Blonder, M. Tinkham, and T. M. Klapwijk, Phys. Rev. B **25**, 4515 (1982).
[12]F. S. Bergeret, A. F. Volkov, and K. B. Efetov, Phys. Rev. B **69**, 174504 (2004); Rev. Mod. Phys. **77**, 1321 (2005).
[13]R. I. Salikhov, I. A. Garifullin, N. N. Garif'yanov, L. R. Tagirov, K. Theis-Bröhl, K. Westerholt, and H. Zabel, Phys. Rev. Lett. **102**, 087003 (2009).
[14]J. Xia, V. Shelukhin, M. Karpovski, A. Kapitulnik, and A. Palevski, Phys. Rev. Lett. **102**, 087004 (2009).
[15]T. Schallenberg and H. Munekata, Appl. Phys. Lett. **89**, 042507 (2006).
[16]H. Munekata, A. Zaslavsky, P. Fumagalli, and R. J. Gambino, Appl. Phys. Lett. **63**, 2929 (1993).
[17]S. Koshihara, A. Oiwa, M. Hirasawa, S. Katsumoto, Y. Iye, C. Urano, H. Takagi, and H. Munekata, Phys. Rev. Lett. **78**, 4617 (1997).
[18]H. Nose, S. Sugahara, and H. Munekata, *Narrow Gap Semiconductors 2007*, edited by B. Murdin and S. Clowes, Springer Proceedings in Physics Vol. 119 (Springer, Dordrecht, 2008).
[19]A. Katz, S. N. G. Chu, B. E. Weir, W. Savin, D. W. Harris, W. C. Dautremont-Smith, T. Tanbun-Ek, and R. A. Logan, J. Vac. Sci. Technol. B **8**, 1125 (1990).
[20]H. Takayanagi and T. Kawakami, Phys. Rev. Lett. **54**, 2449 (1985).
[21]C. Nguyen, J. Werking, H. Kroemer, and E. L. Hu, Appl. Phys. Lett. **57**, 87 (1990).
[22]H. Ohno, H. Munekata, T. Penney, S. von Molnar, and L. L. Chang, Phys. Rev. Lett. **68**, 2664 (1992).
[23]H. Munekata, Mater. Sci. Eng. B **31**, 151 (1995).

[24]F. Matsukura, H. Ohno, A. Shen, and Y. Sugawara, Phys. Rev. B **57**, R2037 (1998).
[25]A. Oiwa, A. Endo, S. Katsumoto, Y. Iye, H. Ohno, and H. Munekata, Phys. Rev. B **59**, 5826 (1999).
[26]G. E. Blonder and M. Tinkham, Phys. Rev. B **27**, 112 (1983).
[27]N. Ashcroft and N. Mermin, *Solid State Physics* (Saunders College, Philadelphia, 1976).
[28]G. A. Khodaparast, J. Kono, Y. H. Matsuda, T. Ikaida, S. Ikeda, N. Miura, T. Slupinski, A. Oiwa, and H. Munekata, *Proceedings of the 26th International Conference on the Physics of Semiconductors*, edited by A. R. Long and J. H. Davies (Institute of Physics Publishing, Bristol, 2003).
[29]P. C. van Son, H. van Kempen, and P. Wyder, Phys. Rev. B **37**, 5015 (1988).
[30]N. Nishizawa, N. Itabashi, T. Akazaki, S. Kobayashi, H. Munekata, and H. Takayanagi, *International Symposium on Quantum Nanostructures and Spin-related Phenomena*, Tokyo, 9-11 March, 2010.
[31]H. Yang, S-H. Yang, S. Takahashi, S. Maekawa, and S. S. P. Parkin, Nat. Mater. **9**, 586 (2010).
[32]R. C. Dynes, V. Narayanamurti, and J. P. Garno, Phys. Rev. Lett. **41**, 1509 (1978).
[33]T. Kiss (private communications).
[34]T. Dietl, H. Ohno, and F. Matsukura, Phys. Rev. B **63**, 195205 (2001).